Friction Analysis of the Motion Suspension System for Improved Space Robot Testing

Ferdinand Elhardt, Anton Shu, Andreas Stemmer, Marco De Stefano, Manfred Schedl, Máximo A. Roa
Institute of Robotics and Mechatronics
German Aerospace Center, DLR
Muenchener Str. 20
82234 Oberpfaffenhofen, Germany
ferdinand.elhardt@dlr.de

Tobias Bruckmann
Chair of Mechatronics
University of Duisburg-Essen
47048 Duisburg, Germany

***Abstract*— Future space missions will require the ability to manipulate satellites for repairing, refueling, and de-orbiting. This makes orbital and planetary space robotic arms a critical technology. Space robotic arms are designed to operate in zero gravity, but are tested on Earth. However, many space robotic arms are non-gravity-bearing and require a gravity support system. For this reason, the Institute of Robotics and Mechatronics at the German Aerospace Center (DLR) and the University of Duisburg-Essen have developed the Motion Suspension System (MSS), a space robot test facility. It is based on a cable-driven parallel robot that allows the space robot arm to operate on ground in the full three-dimensional workspace. To support the robot arm at arbitrary angles, the coupling interface between the MSS and the space robot arm is equipped with two passive joints with angle sensors. Their values are necessary to reconstruct the direction of the applied force, which is used for controller feedback and dynamics analysis of the space robot. As the joints are affected by friction, the measured angle might differ from the real one. This study proposes a experiment-based method to identify the friction. It reveals that the two joints are affected by viscous and static friction (stiction). However, the friction's influence on the performance of the MSS is minor in comparison to other error sources, such as controller and calibration errors. This finding contributes to a more detailed knowledge about the accuracy of the MSS which is important for using it as a verification and validation device for advanced non-gravity-bearing space robot arms.**

TABLE OF CONTENTS

1. INTRODUCTION

As space exploration continues to advance, the ability to manipulate objects in space will become increasingly important for future missions [1]. For this reason, the German Aerospace Center (DLR) has developed the three-meters space robot arm *CAESAR* [2], [3] as presented in Figure 1.

979-8-3503-5597-0/25/$31.00 ©2025 IEEE

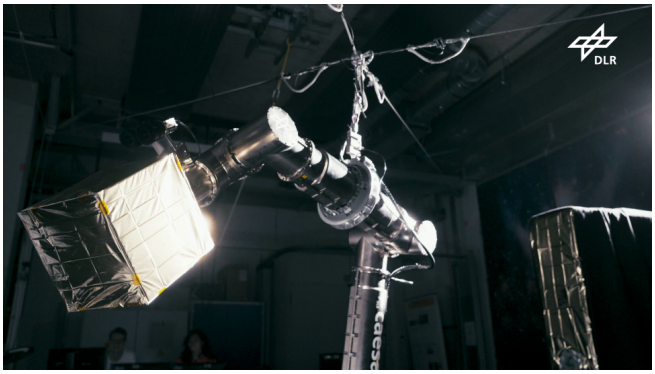

Figure 1. CAESAR (Compliant Assistance and Exploration SpAce Robot) developed by the Institute of Robotics and Mechatronics at DLR uses the MSS as gravitation compensation device for on-ground tests.

As this robot cannot support its own weight on ground, the *Institute of Robotics and Mechatronics* of the DLR and the *University Duisburg-Essen* developed the Motion Suspension System (MSS) (Figure 1) which allows the robot to perform three-dimensional functional motions on Earth.

Key tasks for space robotic manipulators, such as inspecting, repairing, refueling, and safely deorbiting satellites, will require sophisticated robotic capabilities. Robotic manipulators, like those mounted on satellites, will play a vital role in addressing these challenges [4]. For instance, the Canadarm2 [5] robotic arm on the International Space Station has successfully performed a range of tasks, including docking maneuvers, payload handling, and assembly operations. Other flight-proven space manipulators are the ETS-VII manipulator and OEDMS [6]. The reliability of space robotic arms depends on rigorous verification and validation processes to ensure their functionality in space. Since they cannot be modified or repaired after being launched, any design or functional errors must be identified and addressed before. Furthermore, the complexity of robotic operations for on-orbit servicing requires thorough testing and performance evaluation to ensure the robot arm can safely and effectively perform its tasks. Therefore, realistic simulation and testing are essential precursors to deploying a space robotic arm [7].

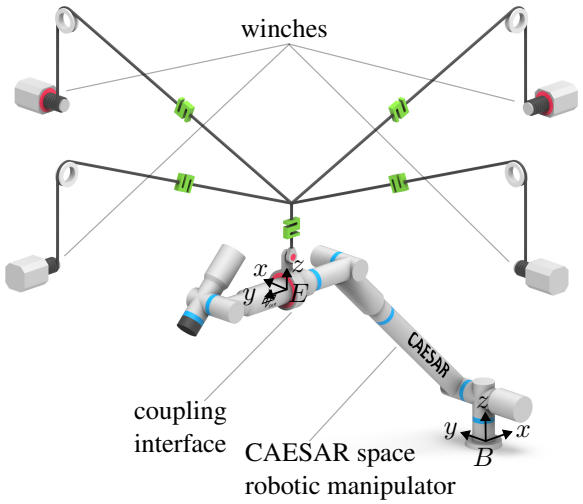

Figure 2. The MSS supports a space robot arm (here the DLR *CAESAR*) for operation and testing on ground. Frame D describes the MSS end effector. Frame B is fixed to the environment.

As most robot arms are designed for zero or low-gravity environments, a significant challenge arises when testing them on Earth: The actuated joints of these robotic arms are typically designed to provide limited torque due to a lightweight design, which is suitable for weightless operations, but can be insufficient to overcome the effects of Earth's gravity. As a result, many robotic arms require additional support mechanisms to operate effectively on ground, which can hinder the accuracy and reliability of on-ground testing and validation [1].

Several mechanisms are available, such as air bearing test facilities which form the most typical test approach of zero-gravity space mechanisms [8], [9], [10]. By using a thin layer of air pressed between the space asset and a flat floor, they create a horizontal zero gravity environment. The *Orbital Robotics Lab* at *ESA ESTEC* [11] is an example of such facility. This method is typically used for testing small satellites, attitude control, and contact-based tasks [12]. This method limits the testing workspace to only horizontal motions. Additionally, this approach is limited by the accuracy of the flatness of the floor [11]. Satellite manufacturers often use helium balloons to qualify the deployment of solar arrays and other mechanisms. Helium balloons are compatible with motions in all six degrees of freedom [13], [14], [15], same as underwater neutral buoyancy tests [16], [17]. However, these approaches are usually avoided due to the high setup effort and the strong hydrodynamic damping effect at fast motions [12]. Free-fall towers and parabolic flight provide actual micro gravity at least for few seconds [18], [19], [20], [21], however, they come with high testing costs and effort. Rail-based suspension systems [1], [22], [23], [24], [25] are usually used for testing the deployment of large structures at satellites, such as solar arrays or antennas. They involve heavy structures and are only suitable for slow motions [26].

The MSS [3], [27], shown in Figures 1 and 2, is a cable-driven parallel robot designed to suspend space robotic arms and reduce the effects of gravity on their joints, considering multiple requirements for such suspension system [28]. Previous experiments with realistic testing trajectories have demonstrated the effectiveness of the MSS in reducing the joint torques of a space robot arm to compensate for gravity [27]. A comparison of joint torques with and without MSS support shows that the necessary space robot joint torques drastically exceed the available torques, indicating that the space robot arm would be unable to operate without the MSS. The study revealed a significant reduction of the space robot torques by a factor of 6 allowing the robot to perform nearly arbitrary motions. Furthermore, the MSS has been successfully tested in complex robotic tasks, including a contact-oriented latching maneuver of a standard interface with positional uncertainties [29]. This showcases the MSS's ability to enable motions in all six degrees of freedom and accurately track the space robot arm's movements, even during small correction motions in impedance control mode. Additionally, the MSS has been shown to adapt to changing payload masses at the space robot's interface [29], highlighting its versatility and reliability in a range of space robotics applications.

While the main effects on the performance of the MSS have been analyzed, such as sensor errors [30] and controller performance [31], this study highlights an additional factor influencing its performance: friction in the joints of the coupling interface between MSS and the space robot arm. The coupling interface, shown in Figure 3, is a rotatable ring that connects the MSS with the space robot arm and provides accurate measurements of its orientation. This work aims to identify friction leading to angle measurement errors, which affect the controller and force analysis, and thus the performance of the MSS as a gravity compensation device.

Modeling friction is a challenging task as it includes a variety of phenomena. In rotational joints, it leads to a torque τ_{fric} acting against the direction of motion which dependents on the material characteristics. At rotating axis, bearings are beneficial to reduce friction. Usually, bigger bearings lead to higher friction due to the larger diameter and hence bigger friction radius. Several models are available to approximate the complex friction behavior. The fundamentals of mathematical friction model were developed by Segner [32] by differentiating between static and dynamic friction. Coulomb found the basic influence factors on friction [33]. One of the earliest friction models by was designed by Dahl [34] and consists of Coulomb and velocity component with a delay when velocity direction changes. The constant friction term is dependent on velocity direction and can be modeled by the non-differentiable $sign()$ function or by the differentiable $tanh()$. Coulomb friction is dependent on the normal forces between two objects and points in the opposite direction of the velocity.

2. SETUP

The MSS is a cable-based parallel robot with four actuators. The operational configuration is shown in Figure 2. Motor-driven winches are connected to four cables. This allows movements in the three-dimensional space and applies the uplift force to the space robot arm. The green force sensors measure the cable forces. By applying a controlled suspension force to the space robot arm, the MSS helps the arm to support the gravitational loads that would otherwise limit its functionality. The system's algorithm computes the optimal suspension forces by solving an optimization problem that minimizes the joint torques of the space robotic arm [38]. The MSS' controller tracks this optimal force. Further details of the MSS are described in the corresponding system paper [27].

The MSS belongs to ground segment equipment and is strictly separated from the space robot arm by using clearly defined interfaces: a communication interface for control signals and a hardware connection for applying the uplift force. Through the communication interface, the space robot continuously requests a desired suspension force [38]. The hardware connection between the MSS and the space robot is located at the coupling frames E, as depicted in Figure 3. At this point, the MSS applies a suspension force in three Cartesian directions represented as ${}_B\boldsymbol{f}_C \in \boldsymbol{R}^3$ with respect to the fixed-base coordinate frame B.

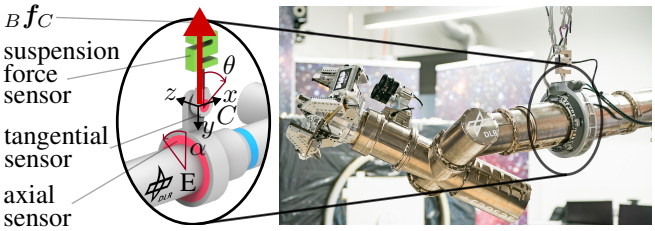

Figure 3. The coupling interface (encircled in black) connects the MSS with the space robot manipulator. It shows the suspension force sensor, the tangential angular sensor, and the axial angular sensor.

The connection is formed as a coupling interface with two passive joints, marked as red circles in Figure 3. The axial joint with the angle α rotates around the tube-shaped robot link with its axis in its center. The tangential joint with the angle θ is attached above the robot link and is oriented tangentially to the tube's axis. Both are located kinematically in series. Ball bearings are used to reduce the friction and the angles are measured by angular sensors. Table 1 presents the properties of the joints and Table 2 details the sensors.

Table 1. Details of the joints and bearings in the coupling interface of the MSS

Joint	***Bearing Type***	***Diameter***
axial	double angular ball bearings	180 mm
tangential	DIN619 ball bearing	9 mm

Table 2. Details of the sensors in the coupling interface of the MSS

Sensor	***Resolution***	***Accuracy***
axial sensor (α)	26 bit	$1.46''$
tangential sensor (θ)	22 bit	$36.0''$
force sensor (f)	24 bit	0.29 N

The measurements from the angle sensors in the coupling interface are crucial for the system performance. The MSS controller utilizes the actual suspension force as a controller feedback, which is reconstructed using data from the angular sensors and other sources [27]. If the values from the angular sensors are compromised, the feedback in the controller is also compromised, resulting in performance degradation of the MSS.

3. METHODS

This section describes the method used to identify the friction in the MSS coupling interface. It covers the performance of the MSS and the approach for identifying the friction.

Performance of the MSS

Previous experiments with the space robot arm *CAESAR* and the MSS have shown that the accuracy of the suspension force exerted by the MSS has a significant impact on the performance of the space robot arm [30]. We define the accuracy of the suspension force as how closely the *actual* suspension force ${}_B\boldsymbol{f}_C$ matches the *desired* suspension force ${}_B\boldsymbol{f}_{C,\text{des}}$. For a realistic testing trajectory, the maximum error in suspension force tracking per direction of the space robot arm is prescribed as less than 9.5 N, which corresponds to a percentage error of less than 3.4 % of the requested suspension force [27]. Step response-based dynamics analysis reveals a linear strongly damped behavior with a rise time of 0.5 s in the horizontal components and a tendency for overshooting in the vertical direction [31].

Sources for Performance Degradation

The reasons for a degraded accuracy of the suspension force are various. On one hand, the computation of the desired suspension force can be compromised by uncertainties in the space robot's kinematic and dynamic models, as well as errors in position measurement. On the other hand, the reconstruction accuracy of the desired suspension force is limited by uncertainties in the forward kinematics and calibration errors of the force and angle sensors. Experimental results have shown that even a small error of 1° can lead to a significant error-induced torque of up to 16 Nm in the space robot joints [30].

Isolation of the MSS Dynamics

In the operational configuration of the MSS and space robot arm, as depicted in Figure 2, the dynamics of the MSS and the space robot arm are interconnected. However, this study focuses on friction only in the MSS. To achieve this, we fix the space robot arm's link to the environment, as shown in Figure 4. The robot arm and its coupling mechanism are positioned at its resting position. This configuration enables the MSS end-effector (point D) to move relative to the space robot arm, but its motion is constrained by the connection cable between points D and E.

Approach for Friction Measurement

This study investigates the friction in the two degrees of freedom of the coupling interface as shown in Figure 3: the axial joint with the angle α and the tangential joint with the angle θ. The approach for the friction estimation is based on correlating the angle and angular velocity with the torque in the joints. We use established friction models for the parameter identification.

To deflect the joints, the angle of the suspension force is changed by adding an input signal in horizontal direction on top of the baseline suspension force ${}_B\boldsymbol{f}_{C,0}$. Figure 5a shows that this causes point D to move horizontally by $\Delta\boldsymbol{x}_{\text{mss}}$. As the robot arm is fixed, this does not lead to a motion of the robotic arm.

The torques on the joints are caused by the pulling force f of the connection cable. These torques – however – are not directly measurable. For this reason, Figure 5 shows

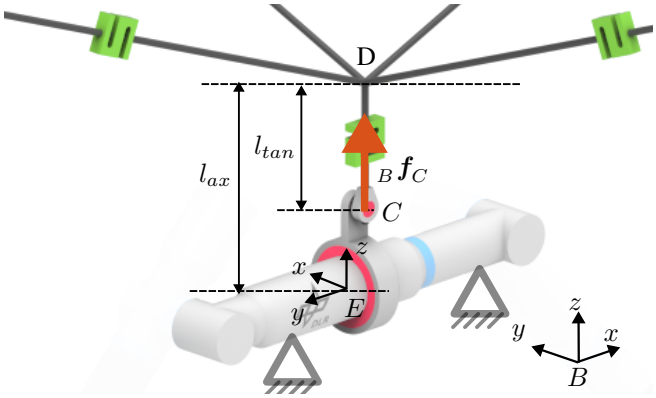

Figure 4. The space robot arm is fixed to the environment in order to decouple the dynamics of the MSS and the robot arm. The configuration is such that the axis of frame E are parallel to frame B.

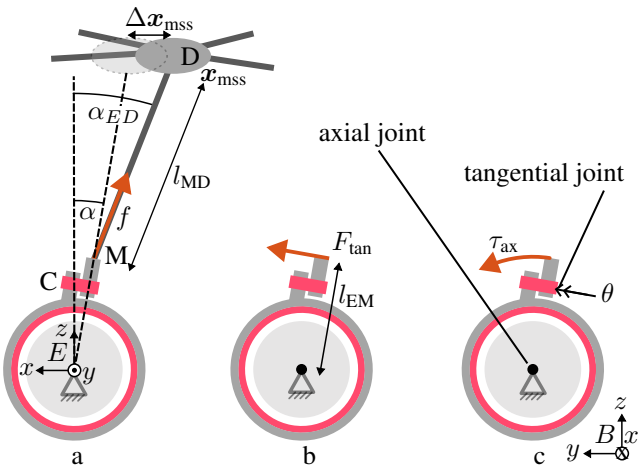

Figure 5. A torque can be applied on the coupling interface if the cable is not aligned with the rotation axis.

the approach of reconstructing the torque τ_{ax} (see (c)) at the example of the axial joint. The same principles apply to the computation for the tangential joint. The reconstruction exploits the geometrical relation in the coupling interface

$$\tau_{\text{ax}} = l_{\text{EM}} F_{\text{tan}} \tag{1}$$

with the length l_{EM} of the lever arm, shown in Figure 5b. The tangential force is computed by

$$F_{\text{tan}} = f \sin(\alpha_{\text{ED}} - \alpha)\cos(\theta) \tag{2}$$

with f being the measured force and α and θ being the measured axial and tangential joint angles, respectively. The $\overline{\text{MD}}$ cable angle α_{ED} needs to be reconstructed as

$$\alpha_{\text{ED}} - \alpha = \text{asin}(\Delta x_{\text{mss},y} / l_{\text{ax}}) \tag{3}$$

with l_{ax} illustrated in Figure 4. The position shift $\Delta x_{\text{mss},y}$ of point D is calculated by using the forward kinematics of the MSS. This detailed setup leads to the applied torque at the joints. To isolate and calculate the frictional component τ_{fric}, we examine the joint's dynamics, using the model

$$\ddot{\alpha} I_{\text{ax}} = \tau_{\text{ax}} - \tau_{\text{ax,fric}} \tag{4}$$

with I_{ax} as the axial inertia of the coupling interface. Note that the joints at the coupling interface do not have any active actuation. Due to slow motions, a quasi-static behavior with $\ddot{\alpha} \approx 0$ is assumed. This leaves with the assumption that friction is the only existing torque in the coupling interface:

$$\tau_{\text{ax}} = \tau_{\text{ax,fric}} \quad . \tag{5}$$

In other words, any deviation between the measured angle α and the reconstructed $\overline{\text{MD}}$ cable angle α_{ED} results from friction. This approach isolates the friction effect.

4. Results

This section shows the results of the friction analysis of the MSS coupling interface. In the configuration shown in Figure 2, the baseline suspension force of the space robot arm is $_B\boldsymbol{f}_{C,0} = [-15.0 \quad 0.2 \quad 334.2]^\intercal$ N, expressed in the fixed frame B. The input signal is added to the baseline suspension force. To test the joints individually, the signal is applied in sequence on the horizontal x and y directions with respect to the coordinate frame B. The change in the suspension force leads to a motion of point D.

These directions of motions correspond to the two coupling interface joints: the motion in direction y leads to a rotation of the axial joint and a motion in x to a rotation of the tangential joint. This results in the two cases: *axial* and *tangential*. As input, a sine signal with an amplitude of 5 N and a frequency of 0.5 Hz is used, resulting in a motion of the MSS end effector point D while point E is fixed.

Figure 6 (top) and 7 (top) show the $\overline{\text{MD}}$ cable angle and measured angle over time of the axial and tangential joint, respectively. The purpose of this figure is to illustrate the impact of friction in the time domain. The input sine signal leads to an amplitude of 0.012 rad joint rotation of both joints (α and θ). The deviation between the $\overline{\text{MD}}$ cable angle and measured values is mainly caused by friction. At the axial joint (Figure 6 top), the observed maximum angular deviation is 0.95×10^{-3} rad at 3.1 s and 4.1 s. This corresponds to an error of 4.3 % with respect to the amplitude. The tangential joint (Figure 7 top) has less deviation: 0.37×10^{-3} rad at 3.3 s and 4.2 s which leads to 1.1 % error. Assuming that friction is the main contributor to the angle deviation (see Equation 4), this observation agrees with the assumption of more friction in the axial bearing due to its size (see Table 1).

Figure 6 (bottom) and 7 (bottom) show the angular velocity and the torque over time of the axial and tangential joint, respectively. It shows that the peak torque on the axial joint is ± 0.089 N m and for the tangential joint ± 0.034 N m. In this experiment, the torque directly correlates with friction, this also indicates that the friction in the axial joint is higher than in the tangential joint. This is expected due to the higher diameter and hence higher friction radius in the axial joint. The direction of the torque changes with the direction of the angular velocity. This is an indicator for viscous or constant friction. Additionally, the torque shows a high gradient when the velocity is zero (see at 2.95 s and 3.95 s). This behavior around velocity zero is an indicator for stiction, which is static friction. Additionally, the torque on the axial joint shows an oscillation behavior with a frequency of about 11.5 Hz. At a first approach, this correlates with the oscillation mode of the coupling interface and cable stiffness.

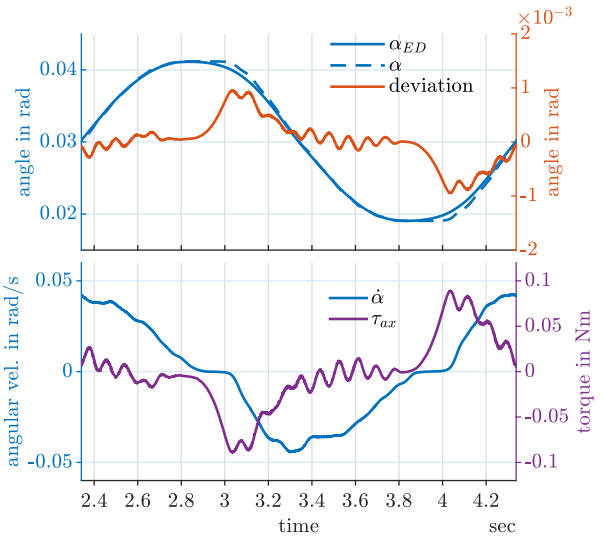

Figure 6. Axial joint; The $\overline{\text{MD}}$ cable angle α_{ED} visibly deviates from the measured angle α (top graph), which indicates friction in the axial joint. The correlation between angular velocity $\dot{\alpha}$ and torque τ_{ax} (bottom graph) shows a torque peak at stillstand indicating that stiction plays a major role in the friction characteristics of the axial joint.

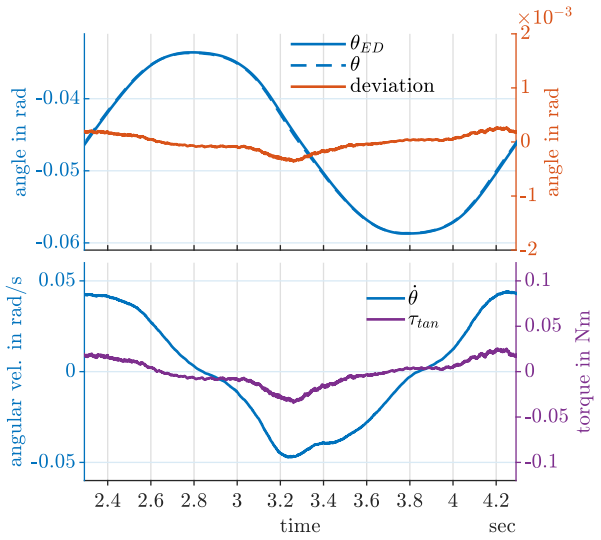

Figure 7. Tangential joint; The $\overline{\text{MD}}$ cable angle θ_{ED} slightly deviates from the measured angles θ due to friction (top graph). The bottom graph shows that torque τ_{tan} increases with higher angular velocity $\dot{\theta}$.

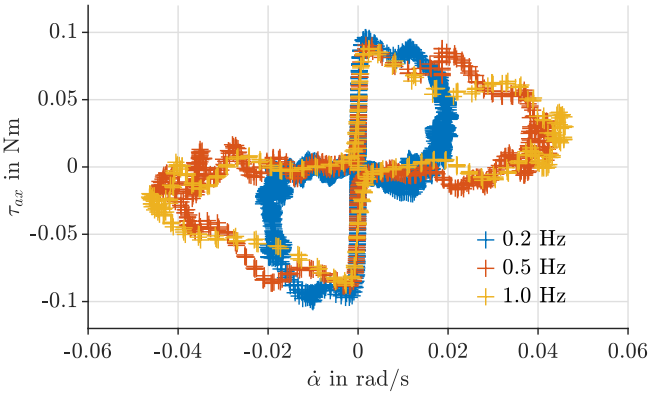

Figure 8. Axial joint; the relation between angular velocity $\dot{\alpha}$ and torque τ_{ax} for multiple frequencies of the sine input signal shows repeatably an increasing torque around zero velocity. This is typical for the break-through torque of the stiction type of friction.

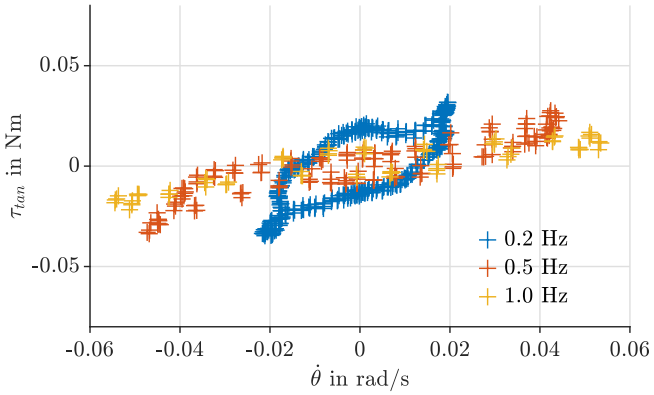

Figure 9. Tangential joint; velocity $\dot{\theta}$ and torque τ_{tan} for multiple frequencies of the sine input signal show a typical characteristic for viscous friction.

Figure 8 and 9 include multiple experiments with varying frequency of the input sine signal. They show the angular velocity and the torque of the axial and tangential joint, respectively. The angular velocity is limited at $\pm \approx 0.05\,\text{rad}\,\text{s}^{-1}$ which is caused by the maximum controller velocity. The experiment with the $0.2\,\text{Hz}$ sine input signal is even slower. The results are summarized in Table 3 and explained in detail in the following.

Let us focus on the axial joint (Figure 8), which consists of the bigger bearing. It shows that the torque increases until it reaches the break-through level before the joint starts moving. This torque at velocity zero corresponds to a stiction-based break-through torque of $0.089\,\text{N}\,\text{m}$. Stiction is the main driver for friction in this case. The graph also shows a strong symmetric hysteresis behavior. With higher angular velocity, the torque decreases to 0. This is due to an underlying constant friction term which adds up with the acceleration of the inertia. The deceleration phase comes with a torque value close to $0\,\text{N}\,\text{m}$. This is explained with the fact that the constant friction cancels out the inertia's deceleration torque.

The tangential joint (Figure 9) is equipped with the smaller bearing. Its friction is characterized as a linear viscous friction coefficient of $0.40\,\text{N}\,\text{m}\,\text{rad}^{-1}\,\text{s}$. This describes an approximate linear correlation between torque and angular velocity. The maximum friction torque is significantly less than the axial joint. This agrees with the assumption that a smaller bearing leads to less friction. The experiment with the $0.2\,\text{Hz}$ sine input signal exhibits more complex frictional

behavior. A hysteresis is visible and the friction coefficient is higher. As the velocity oscillates, the torque does not respond instantaneously, causing the elliptical shape. This could be due to more variability in the frictional forces at low frequencies, possibly due to stick-slip behavior or static friction effects dominating at lower velocities.

Table 3. Friction results of the parameter analysis focusing on the two passive joints of the MSS coupling interface.

	axial joint	***tangential joint***
break-through torque	$0.089\,\mathrm{N\,m}$	$\approx 0\,\mathrm{N\,m}$
viscous coefficient	$\approx 0\,\mathrm{N\,m\,rad^{-1}\,s}$	$0.40\,\mathrm{N\,m\,rad^{-1}\,s}$

5. DISCUSSION

The results indicate that the two joints in the MSS coupling interface are subject to friction, which has implications for the system performance. The angular measurement of the coupling interface is a critical component in reconstructing the suspension force which in turn is an important feedback signal for the MSS controller. However, if the reconstructed suspension force is compromised due to friction, it can lead to a degradation in the overall performance of the MSS. This section will examine the impact of identified friction on the MSS's performance, highlighting its effects on the system's overall behavior.

The findings reveal distinct behavior in the coupling interface of the MSS, with notable differences between the axial (α) and tangential (θ) joint axes (see Figure 3). Specifically, the axial direction exhibits stiction, whereas the tangential joint is characterized by viscous friction. Furthermore, the axial friction leads to greater angle deviations compared to the tangential joint. This disparity in friction behavior has implications for the accuracy of the suspension force, with degradation being more pronounced in the x direction of the coupling frame E. Consequently, when assessing the suspension force error due to friction in the fixed base frame B, it is essential to consider the configuration of the robotic arm, as this will impact the magnitude of the error.

The stiction type of friction has a distinct effect on the MSS performance. Due to stiction, the integrated angular sensor is unable to measure motions below the break-through torque, resulting in an inability to detect small changes in the suspension force. Consequently, the MSS controller is unable to accurately track these changes, leading to a tracking error. In an attempt to compensate, the controller might increase its output, which can result in a sudden and excessive motion, manifesting as overshooting. This, in turn, can lead to a corrective motion by the controller, causing an opposite motion that may ultimately destabilize the system. To mitigate this effect, the controller must be carefully tuned to account for the stiction phenomenon, or an observer can be implemented to mitigate the measurement error.

Friction is one of several key factors influencing the MSS performance, alongside sensor errors and controller performance. To gauge the relative impact of friction on the system performance, we must consider its contribution in the context of other error sources. Table 4 provides a comprehensive overview of the possible error sources affecting the MSS performance, taking previous studies into account. Calibration errors lead to $16\,\mathrm{N\,m}$ error on the space robot joints while the controller performance is velocity dependent. Upon comparison, it becomes clear that friction plays a relatively minor role. However, it contributes to the error from the controller as it alters the input signal. Consequently, when prioritizing performance improvements, attention should be focused on the other factors, which have a more significant impact on the overall system performance.

Despite the impact of friction being minor compared to other effects, there are several mitigation strategies to reduce its effect on MSS performance. Firstly, the hardware can be improved by incorporating bearings with reduced friction. Secondly, multiple sensor or observation values can be used to improve the reconstruction of the suspension force. Specifically, the motion of point D can be included in the reconstruction strategy, which can be measured using the MSS forward kinematics, inertial measurement units, or external measurement methods. By combining these measurements, Kalman filters can be employed to improve the accuracy and robustness of the suspension force reconstruction.

6. CONCLUSION

This study investigates the frictional effects of the MSS coupling mechanism and shows their impact on the MSS performance. Specifically, the axial joint is predominantly affected by stiction while in contrast the tangential joint is primarily influenced by viscous friction. These findings provide insight into the sources of measurement degradation, however, other error sources such as calibration errors or controller performance have a higher effect on the MSS overall performance. Future research directions should focus on identifying and mitigating additional error sources that impact the performance of the MSS. Specifically, the performance of MSS actuators and winches can be subject of further investigation. To measure the error due to friction during operation, researchers can explore sensor fusion approaches that incorporate additional positional information such as the forward kinematics of the MSS. Feed-forward methods can help to mitigate the effect of friction. Moreover, mechanical improvements to joints and bearings can be implemented to reduce friction and enhance overall system performance. These efforts will help to refine the MSS's accuracy and reliability paving the way for using the MSS as verification and validation device for advanced non-gravity-bearing space robot arms.

Table 4. Overview of error sources for the MSS and its implication on the performance

error source	***error***	***impact on space robot*** [30]	***source***
calibration uncertainty	angle error $1.0°$	$16\,\mathrm{N\,m}$	[30]
controller performance	step response rise time of $\sim 0.6\,\mathrm{s}$	velocity-dependent	[31]
joint friction	angle error $0.054°$	$0.86\,\mathrm{N\,m}$	this study

REFERENCES

[1] E. Papadopoulos, F. Aghili, O. Ma, and R. Lampariello, "Robotic Manipulation and Capture in Space: A Survey," in *Frontiers in Robotics and AI*, 2021. DOI: 10.3389/frobt.2021.686723.

[2] A. Beyer, G. Grunwald, M. Heumos, M. Schedl, R. Bayer, W. Bertleff, B. Brunner, R. Burger, J. Butterfaß, R. Gruber, T. Gumpert, F. Hacker, E. Krämer, M. Maier, S. Moser, J. Reill, M. A. Roa, H.-J. Sedlmayr, N. Seitz, and A. Albu-Schäffer, "CAESAR: Space Robotics Technology for Assembly, Maintenance, and Repair," in *Proc. Int. Astronautical Congress*, Bremen, 2018.

[3] F. Elhardt, M. Ekal, M. A. Roa, R. Bayer, A. Beyer, B. Brunner, M. De Stefano, S. Moser, Schedl Manfred, H.-J. Sedlmayr, Stelzer Martin, A. Stemmer, B. Thomas, R. Burger, J. Butterfass, T. Gumpert, F. Hacker, E. Krämer, J. Reill, N. Seitz, T. Wimmer, R. Boumann, T. Bruckmann, R. Heidel, P. Lemmen, W. Bertleff, J. Heindl, D. Reintsema, F. Steinmetz, G. Grunwald, G. Hirzinger, K. Landzettel, and A. Albu-Schäffer, "Video: DLR's Advancements in Space Robotic Manipulation," presented at the 40th Anniversary of the IEEE Conference on Robotics and Automation, Rotterdam, 2024.

[4] R. H. Miller, M. L. Minsky, and D. B. S. Smith, "Space Applications of Automation, Robotics and Machine Intelligence Systems (ARAMIS). Volume 4: Supplement, Appendix 4.3: Candidate ARAMIS Capabilities," NASA, NAS 1.26:162083, 1982.

[5] G. Gibbs and S. Sachdev, "Canada and the International Space Station program: Overview and status," *Acta Astronautica*, vol. 51, no. 1, pp. 591–600, 2002. DOI: 10.1016/S0094-5765(02)00077-2.

[6] T. Rybus, "Robotic manipulators for in-orbit servicing and active debris removal: Review and comparison," *Progress in Aerospace Sciences*, vol. 151, p. 101 055, 2024. DOI: 10.1016/j.paerosci.2024.101055.

[7] M. De Stefano, H. Mishra, A. M. Giordano, R. Lampariello, and C. Ott, "A Relative Dynamics Formulation for Hardware-in-the-Loop Simulation of On-Orbit Robotic Missions," *IEEE Robotics and Automation Letters*, 2021. DOI: 10.1109/LRA.2021.3064510.

[8] H. Kolvenbach and K. Wormnes, "Orbit - A Facility for Experiments on Free Floating Contact Dynamics," in *Proc. Symp. on Advanced Space Technologies in Robotics and Automation (ASTRA)*, Netherlands: ESA, 2015.

[9] E. Papadopoulos, I. Paraskevas, T. Flessa, K. Nanos, Y. Rekleitis, and I. Kontolatis, "The NTUA Space Robot Simulator: Design & Results," in *Proc. ESA Workshop on Advanced Space Technologies for Robotics and Automation*, 2008.

[10] J. L. Schwartz, M. A. Peck, and C. D. Hall, "Historical Review of Air-Bearing Spacecraft Simulators," *J. of Guidance, Control, and Dynamics*, 2003. DOI: 10.2514/2.5085.

[11] H. Kolvenbach and K. Wormnes, "Recent Developments on On-Orbit, a 3-DOF Free Floating Contact Dynamics Testbed," in *Proc. Int. Symp. on Artificial Intelligence, Robotics and Automation in Space (i-SAIRAS)*, Beijing, China, 2016.

[12] A. Flores-Abad, O. Ma, K. Pham, and S. Ulrich, "A review of space robotics technologies for on-orbit servicing," *Progress in Aerospace Sciences*, 2014. DOI: 10.1016/j.paerosci.2014.03.002.

[13] M. Leipold, M. Eiden, C. Garner, L. Herbeck, D. Kassing, T. Niederstadt, T. Krüger, G. Pagel, M. Rezazad, H. Rozemeijer, W. Seboldt, C. Schöppinger, C. Sickinger, and W. Unckenbold, "Solar sail technology development and demonstration," *Acta Astronautica*, vol. 52, no. 2-6, pp. 317–326, 2-6 2003. DOI: 10.1016/S0094-5765(02)00171-6.

[14] L. Herbeck, M. Leipold, C. Sickinger, M. Eiden, and W. Unckenbold, "Development and Test of Deployable Ultra-Lightweight CFRP-Booms for a Solar Sail," *Spacecraft Structures, Materials and Mechanical Testing*, ESA Special Publication, vol. 468, C. Stavrinidis, A. Rolfo, and E. Breitbach, Eds., p. 107, 2001.

[15] O. Han, D. Kienholz, P. Janzen, and S. Kidney, "Gravity-Offloading System for Large-Displacement Ground Testing of Spacecraft Mechanisms," in *Proc. Aerospace Mechanisms Symp.*, 2010.

[16] C. Carignan and D. Akin, "The reaction stabilization of on-orbit robots," *IEEE Control Systems Magazine*, 2000. DOI: 10.1109/37.887446.

[17] H. Sawada, K. Ui, M. Mori, H. Yamamoto, R. Hayashi, S. Matunaga, and Y. Ohkami, "Micro-gravity experiment of a space robotic arm using parabolic flight," *Advanced Robotics*, 2004. DOI: 10.1163/156855304322972431.

[18] C. Lotz, Y. Wessarges, J. Hermsdorf, W. Ertmer, and L. Overmeyer, "Novel active driven drop tower facility for microgravity experiments investigating production technologies on the example of substrate-free additive manufacturing," *Advances in Space Research*, vol. 61, no. 8, pp. 1967–1974, 8 2018. DOI: 10.1016/j.asr.2018.01.010.

[19] C. Menon, A. Aboudan, S. Cocuzza, A. Bulgarelli, and F. Angrilli, "Free-Flying Robot Tested on Parabolic Flights: Kinematic Control," *Journal of Guidance, Control, and Dynamics*, vol. 28, no. 4, pp. 623–630, 4 2005. DOI: 10.2514/1.8498.

[20] J. F. Lekan, E. S. Neumann, and D. M. Thompson, *Ground-Based Reduced-Gravity Facilities*, 1998.

[21] C. Lotz, B. Piest, E. Rasel, and L. Overmeyer, "The Einstein Elevator: Space Experiments at the new Hannover Center for Microgravity Research," *Europhysics News*, vol. 54, no. 2, pp. 9–11, 2 2023. DOI: 10.1051/epn/2023201.

[22] M. Deremetz, M. Debroise, S. Govindaraj, A. But, I. Nieto, M. De Stefano, H. Mishra, B. Brunner, G. Grunwald, M. A. Roa, M. Reiner, M. Závodník, M. Komarek, J. D'Amico, F. Cavenago, J. Gancet, P. Letier, M. Ilzkovitz, L. Gerdes, and M. Zwick, "Demonstrator Design of a modular Multi-Arm Robot for on-orbit large Telescope Assembly," in *Proc. Symp. on Advanced Space Technologies in Robotics and Automation*, Noordwijk, Netherlands, 2022.

[23] Brown and J. Dolan, "A Novel Gravity Compensation System for Space Robots," in *Proc. ASCE Specialty Conf. on Robotics for Challenging Environments*, 1994.

[24] L. K. Dungan, P. S. Valle, D. R. Bankieris, A. P. Lieberman, L. Redden, and C. Shy, "Patent: US9194977B1. Active response gravity offload and method," U.S. Patent 9194977B1, 2015.

[25] X. Ding, Y. Wang, Y. Wang, and K. Xu, "A review of structures, verification, and calibration technologies of space robotic systems for on-orbit servicing," *Science China Technological Sciences*, 2020. DOI: 10.1007/s11431-020-1737-4.

[26] G. White and Yangsheng Xu, "An active vertical-direction gravity compensation system," *IEEE Trans. on Instrumentation and Measurement*, vol. 43, no. 6, pp. 786–792, 6 1994. DOI: 10.1109/19.368066.
[27] F. Elhardt, R. Boumann, M. De Stefano, R. Heidel, P. Lemmen, M. Heumos, C. Jeziorek, M. A. Roa, M. Schedl, and T. Bruckmann, "The Motion Suspension System – MSS: A Cable-Driven System for On-Ground Tests of Space Robots," in *Advances in Mechanism and Machine Science*, M. Okada, Ed., vol. 148, Cham: Springer Nature, 2023, pp. 379–388. DOI: 10.1007/978-3-031-45770-8_38.
[28] F. Elhardt, R. Boumann, M. De Stefano, R. Heidel, P. Lemmen, M. Heumos, C. Jeziorek, M. Roa, M. Schedl, and T. Bruckmann, "System Requirements Elicitation and Conceptualization for a Novel Space Robot Suspension System," in *Proc. Symp. on Advanced Space Technologies in Robotics and Automation (ASTRA)*, Leiden, Niederlande, 2023.
[29] F. Elhardt, M. De Stefano, M. Schedl, M. Stelzer, A. Stemmer, I. Rodriguez, R. Vijayan, M. A. Roa, and T. Bruckmann, "The Motion Suspension System for On-Ground Tests of Space Robots: Demonstration and Results," in *2024 IEEE Aerospace Conference*, Big Sky, MT, USA: IEEE, 2024, pp. 1–9. DOI: 10.1109/AERO58975.2024.10521208.
[30] F. Elhardt, M. De Stefano, M. Schedl, A. Stemmer, T. Bruckmann, and M. A. Roa, "Analysis of Sensor Errors of a Suspension Systems for Space Robots," in *Proc. International Conference on Space Robotics*, Luxembourg, 2024.
[31] F. Elhardt, A. Stemmer, A. Shu, M. De Stefano, M. Schedl, M. A. Roa, and T. Bruckmann, "Experiment-Based Performance Analysis of the Motion Suspension System for Space Robot Testing," in *Proc. 75th International Astronautical Congress*, Milan, Italy, 2024.
[32] D. Dowson, *History of Tribology*, 2. ed. London: Professional Engineering Publishing, 1998, 768 pp.
[33] E. Popova and V. L. Popov, "The research works of Coulomb and Amontons and generalized laws of friction," *Friction*, vol. 3, no. 2, pp. 183–190, 2015. DOI: 10.1007/s40544-015-0074-6.
[34] P. R. Dahl, "A Solid Friction Model," Fort Belvoir, VA: Defense Technical Information Center, 1968. DOI: 10.21236/ADA041920.
[35] R. Stribeck, *Kugellager für beliebige Belastungen*. Springer, 1901, 73 pp. Google Books: zEbbMAAACAAJ.
[36] C. Makkar, W. Dixon, W. Sawyer, and G. Hu, "A new continuously differentiable friction model for control systems design," in *Proceedings, 2005 IEEE/ASME International Conference on Advanced Intelligent Mechatronics.*, 2005, pp. 600–605. DOI: 10.1109/AIM.2005.1511048.
[37] M. Iskandar and S. Wolf, "Dynamic friction model with thermal and load dependency: Modeling, compensation, and external force estimation," in *2019 International Conference on Robotics and Automation (ICRA)*, 2019, pp. 7367–7373. DOI: 10.1109/ICRA.2019.8794406.
[38] M. De Stefano, R. Vijayan, A. Stemmer, F. Elhardt, and C. Ott, "A Gravity Compensation Strategy for On-ground Validation of Orbital Manipulators," in *Proc. IEEE Int. Conf. on Robotics and Automation*, London, UK, 2023.

BIOGRAPHY

Ferdinand Elhardt *earned a Master's in Mechanical Engineering from TUM, Munich. After researching robotic locomotion at Oxford Robotics Institute, he joined DLR's Robotics and Mechatronics Institute in 2021. His PhD, in partnership with the University of Duisburg-Essen, focuses on testing space robots on ground. He is responsible for the Motion Suspension System and conducts research on space robot verification and qualification.*

Anton Shu *Anton Shu holds a B.Sc. in Mechatronics and Information Technology from the Technical University of Munich, Germany, awarded in 2014, and an M.Sc. in Mechanical Engineering from the same institution, awarded in 2018. He has been with the German Aerospace Center (DLR), Institute of Robotics and Mechatronics, Wessling, Germany, since that time.*

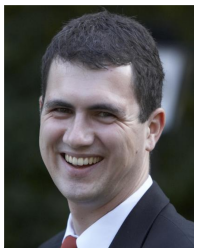

Andreas Stemmer *graduated in Electrical Engineering and Information Technology with major subject Control Theory and Automation Engineering at the Technical University Munich in 2005. He wrote his diploma thesis at the German Aerospace Center (DLR) where he since then works as research engineer. His main fields of interest include software and firmware development, as well as joint level control for terrestrial and space robots.*

Marco De Stefano *received his bachelor degree in aerospace engineering (2008) and his master's degree cum laude in astronautical engineering (2011) from Sapienza, University of Rome. In 2019, he received his PhD (summa cum laude) from the University of Modena and Reggio Emilia, which was recognized as finalist for the 2020 Georges Giralt PhD Award. Since 2012, he is a researcher with DLR, heading the Flying and Floating-base robot control group since 2023 with main focus on space robot dynamics, control theory, and hardware-in-the-loop simulation.*

Manfred Schedl *received his diploma from the Technical University of Munich. Since 1987, he has been with the Institute of Robotics and Mechatronics at the German Aerospace Center (DLR). He contributed to several space missions, especially ROTEX, ROKVISS, MASCOT and MMX. His experience is in Robotics, Sensor- and Drive-Technology for terrestrial and space applications.*

Máximo A. Roa *received his doctoral degree in 2009 from Universitat Politecnica de Catalunya (UPC), and the Project Management Professional (PMP) Certification in 2016. He worked for Hewlett Packard R&D before joining the Institute of Robotics and Mechatronics of the German Aerospace Center (DLR) in 2010 as Senior Research Scientist, leading the group on Robotic Planning and Manipulation.*

Tobias Bruckmann *is a senior researcher, lecturer and professor for mechatronics at the University of Duisburg-Essen. His research interests include robotics, automation technology, and human machine interfaces. He has organized and participated in numerous conferences and workshops in the fields of mechatronics and robotics. He has also been involved in several research projects, including the development of a cable-driven parallel robot for use in the construction industry.*